

Structural Evolution of Colloidal Gels During Constricted Microchannel Flow

Jacinta C. Conrad^{*,†,‡} and Jennifer A. Lewis^{†,‡,§}[†]Frederick Seitz Materials Research Laboratory, [‡]Materials Science and Engineering Department, and [§]Chemical and Biomolecular Engineering Department, University of Illinois, Urbana, Illinois 61801

Received January 2, 2010. Revised Manuscript Received March 8, 2010

We investigate the structure of colloidal gels flowing through constrictions in microchannels using confocal microscopy. As the gel traverses the constricted region, both the average velocity and particle density increase downstream. While the average flow profile is smoothly varying, stagnation zones develop at the constriction entry, leading to markedly nonuniform local flow profiles. Dense clusters undergo shear-induced yielding at intercluster boundaries, which enhances the structural heterogeneity of the suspension at the constriction outlet.

Introduction

The flow of colloidal suspensions within confined geometries is ubiquitous, with examples ranging from blood flow through vascular networks^{1–3} to material assembly methods such as inkjet printing^{4,5} and direct-write assembly.^{6–9} Recent experiments have quantified the flow profiles of suspensions in uniform microchannels using microparticle imaging velocimetry,^{3,10} fluorescence correlation spectroscopy,¹¹ and nuclear magnetic resonance imaging.^{12–14} However, those techniques do not provide information about suspension structure during flow. Quite recently, the structural evolution of aggregates during constricted flow has been characterized by small-angle light scattering.¹⁵ However, this approach does not permit the measurement of the flow profiles. New investigations are therefore needed to correlate constricted flow behavior simultaneously with suspension structure, which are both of fundamental^{16,17} and technological interest.¹⁸

One powerful technique for exploring the relationship between structure and flow behavior in colloidal suspensions is confocal microscopy.¹⁹ By directly imaging particles during flow, both local flow profiles and particle distributions can be readily

accessed.²⁰ For example, confocal microscopy has recently been used to investigate the flow behavior of colloidal suspensions in uniform microchannels, including shear-induced migration in colloidal fluids,^{21–23} wall slip,²⁴ velocity oscillations²⁵ in colloidal glasses, and both shear-²⁶ and field-induced²⁷ restructuring in colloidal gels. Surprisingly, despite the capabilities afforded by this technique, the effects of channel geometry on the structure and flow properties of attractive suspensions have yet to be explored.

In this letter, we investigate the structural evolution of colloidal gels flowing through a constricted microchannel using confocal microscopy. As a benchmark, the gel structure is first characterized in the quiescent state. As the suspension flows through the constriction, its average velocity increases downstream because of the conservation of flux. In addition, the concentration of particles increases downstream from the constriction, revealing that filter pressing of the particles occurs because of differential flow with the liquid. These changes indicate that flow through the constriction leads to restructuring in the suspension. Locally, shear stresses lead to the formation of dense clusters that yield at intercluster boundaries. Near the constriction entrance, regions of slow velocity develop in which particles transiently jam and unjam via formation and yielding of particle bonds; the duration of the transient jams decreases with increasing applied pressure. The continuous yielding and reforming of both interparticle and intercluster bonds provides a mechanism for long-length-scale structural changes, which are quantified by the number density fluctuations. When the applied pressure is sufficiently low, the suspension structure near the midplane of the microchannel exhibits features characteristic of a connected gel network. However, relative to the quiescent state, the number density fluctuations are enhanced near the walls of the channel, where shear-induced structural changes are most pronounced. Our observations provide insight into the mechanisms by which constricted flow induces structural and dynamical changes within attractive colloidal suspensions and are directly relevant to the design of nozzle and die geometries for direct-write assembly and extrusion, respectively.

(21) Frank, M.; Anderson, D.; Weeks, E. R.; Morris, J. F. *J. Fluid Mech.* **2003**, *493*, 363.

(22) Semwogerere, D.; Morris, J. F.; Weeks, E. R. *J. Fluid Mech.* **2007**, *581*, 437.

(23) Semwogerere, D.; Weeks, E. R. *Phys. Fluids* **2008**, *20*, 043306.

(24) Isa, L.; Besseling, R.; Poon, W. C. K. *Phys. Rev. Lett.* **2007**, *98*, 198305.

(25) Isa, L.; Besseling, R.; Morozov, A. N.; Poon, W. C. K. *Phys. Rev. Lett.* **2009**, *102*, 058302.

(26) Conrad, J. C.; Lewis, J. A. *Langmuir* **2008**, *24*, 7628.

(27) Kogan, M.; Solomon, M. J. *Langmuir* **2010**, *26*, 1207.

*Corresponding author. E-mail: jconrad@uh.edu.

(1) Ku, D. N. *Annu. Rev. Fluid Mech.* **1997**, *29*, 399.

(2) Lima, R.; Wada, S.; Tanaka, S.; Takeda, M.; Ishikawa, T.; Tsubota, K.-I.; Imai, Y.; Yamaguchi, T. *Biomed. Microdev.* **2008**, *10*, 153.

(3) Lima, R.; Wada, S.; Tsubota, K.; Yamaguchi, T. *Meas. Sci. Technol.* **2006**, *17*, 797.

(4) Sachs, E.; Cima, M.; Williams, P.; Brancazio, D.; Cornie, J. *J. Eng. Ind.* **1992**, *114*, 481.

(5) Park, J.; Moon, J. *Langmuir* **2006**, *22*, 3506.

(6) Park, J.; Moon, J.; Shin, H.; Wang, D.; Park, M. *J. Colloid Interface Sci.* **2006**, *298*, 713.

(7) Smay, J. E.; Gratson, G. M.; Shepherd, R. F.; Cesarano, J., III; Lewis, J. A. *Adv. Mater.* **2002**, *14*, 1279.

(8) Lewis, J. A. *Adv. Funct. Mater.* **2006**, *16*, 2193.

(9) Rao, R. B.; Krafcik, K. L.; Morales, A. M.; Lewis, J. A. *Adv. Mater.* **2005**, *17*, 289.

(10) Roberts, M. T.; Mohraz, A.; Christensen, K. T.; Lewis, J. A. *Langmuir* **2007**, *23*, 8726.

(11) Hashmi, S. M.; Loewenberg, M.; Dufresne, E. R. *Opt. Exp.* **2007**, *15*, 6528.

(12) Moraczewski, T.; Shapley, N. C. *Phys. Fluids* **2007**, *19*, 103304.

(13) Xi, C.; Shapley, N. C. *J. Rheol.* **2008**, *52*, 625.

(14) Iwamiya, J. H.; Chow, A. W.; Sinton, S. W. *Rheol. Acta* **1994**, *33*, 267.

(15) Soos, M.; Ehrh, L.; Bäßler, M. U.; Morbidelli, M. *Langmuir* **2010**, *26*, 10.

(16) Denn, M. M. *Annu. Rev. Fluid Mech.* **2001**, *33*, 265.

(17) Haw, M. D. *Phys. Rev. Lett.* **2004**, *92*, 185506.

(18) Biesheuvel, P. *Chem. Eng. Sci.* **2000**, *55*, 2595.

(19) Prasad, V.; Semwogerere, D.; Weeks, E. R. *J. Phys.: Condens. Matter* **2007**, *19*, 113102.

(20) Besseling, R.; Isa, L.; Weeks, E. R.; Poon, W. C. K. *Adv. Colloid Interface Sci.* **2009**, *146*, 1.

Experimental Methods

Materials System. Fluorescent-core silica microspheres are synthesized using a modified Stöber process²⁸ and are repeatedly washed in ethanol and doubly deionized water at pH 6 to remove excess reagents. Their radius a is 430 ± 30 nm, as measured by scanning electron microscopy (6060LV, JEOL, Tokyo, Japan), and their density is 1.94 g/mL. Prior to polyelectrolyte adsorption, the microspheres are first suspended in pH 6 doubly deionized water and diluted to a volume fraction ϕ of 0.05. A cationic polyelectrolyte, poly(ethylenimine) (PEI, $M_w = 1800$, Polysciences, Inc., Warrington, PA), is then added to the colloidal suspension in a ratio of 2.5 mg of PEI per m^2 of silica. After PEI adsorption, the zeta potential of the coated microspheres is 55 ± 3 mV. To match the refractive index, the microspheres are transferred to a 2:1 v/v solution of dimethylsulfoxide (DMSO, Fisher Chemical, Fairlawn, NJ) and doubly deionized water at pH 6 ($\rho_{\text{DMSO-H}_2\text{O}} = 1.084$ g/mL) and then concentrated by sedimentation.

To induce attraction between the PEI-coated microspheres, an anionic polyelectrolyte, poly(acrylic acid) (PAA, $M_w = 2000$, Aldrich, St. Louis, MO), is added at a ratio of 1:2 [COONa]/[NH₂], which indicates the number of ionizable carboxylate and amine groups present along the PAA and PEI backbones, respectively.^{29,30} The PAA solution is added in four aliquots to the suspension, which is vortex mixed for ~ 1 s after each addition. Although the attractive strength between particles induced by polyelectrolyte bridging is not directly quantified, the quiescent morphology of these colloidal gels²⁶ is reminiscent of that observed in depletion gels with a short-range attraction³¹ whose strength is on the order of tens of $k_B T$ s.³²

Device Fabrication. The microchannel devices for these experiments are fabricated using standard soft-lithography techniques.³³ Briefly, silicon wafers are first patterned with the SU-8 photoresist (SU-8 100, Microchem, Newton, MA) and used as masters from which poly(dimethylsiloxane) (PDMS, Sylgard 184, Dow Corning, Midland, MI) devices are templated. The devices are mounted onto $48 \text{ mm} \times 65 \text{ mm}$ coverslips (Thermo Scientific cover glass 3335, Fisher Scientific, Pittsburgh, PA). Schematically, the microchannel narrows from an inlet of width D to an outlet of width d through a constriction with an opening angle of α , as shown in Figure 1. In our experiments, the outlet width $d = 50 \mu\text{m}$ is held constant. We investigated the flow and structure in devices with two different inlet widths, $D = 100$ and $150 \mu\text{m}$, giving turndown ratios of $D/d = 2$ and 3, respectively, and two opening angles, $\alpha = 27$ and 72° . The lengths of the inlet and outlet channels are 2.5 ± 0.2 and 2 ± 0.2 cm, respectively, and the channel height is $40 \pm 2 \mu\text{m}$.

Polyethylene tubing (Intramedic PE10, BD, Franklin Lakes, NJ) with an inner diameter of 0.28 mm and a length of 15 cm is used to transport the suspension into the device. A pressure applied across the device via a custom-built pressure box drives the flow of the colloidal suspension through the microchannel. For the experiments discussed herein, the minimum and maximum applied pressures are 0.7 and 7 kPa, respectively.

Confocal Microscopy. We directly image both quiescent and flowing suspensions at two volume fractions ($\phi = 0.26$ and 0.30) using confocal laser scanning microscopy. The structure and flow behavior exhibited by each suspension is qualitatively similar. However, clogging frequently disrupts the suspension flow for the more concentrated system even when the applied pressure is relatively high. We therefore report results only for $\phi = 0.26$. Images are acquired with a Vt-eye confocal (Visitech, Sunderland, U.K.) attached to an Olympus microscope with a $100\times$ objective

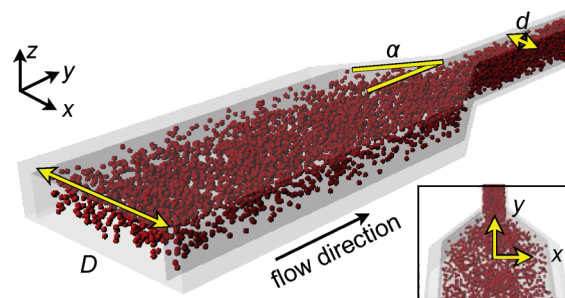


Figure 1. Schematic illustration of the constriction flow experiments. The channel narrows from an input width, D , to an output width, d , through a constriction with angle α . (Inset) View of the schematic in the x - y plane showing the origin of the coordinate axes used in this study: $x = 0$ at the midpoint of the channel region, $y = 0$ immediately before the constriction entrance, and $z = 0$ at the bottom plane of the microchannel.

lens (N.A. = 1.32). To characterize the structure of quiescent suspensions, we acquire 3D image stacks in large sample chambers; the frame rate for a 2D image is ~ 2 frames/s, and the vertical spacing between consecutive images is $0.1 \mu\text{m}$. The high flow rates of flowing suspensions preclude 3D imaging of individual colloids. To characterize the structure and velocity profile of suspensions flowing through constrictions, we therefore acquire a 2D image series at a frame rate of 30 frames/s. At each pressure, 1000 images are taken at heights ranging from 3 to $30 \mu\text{m}$ above the bottom surface of the microchannel.

Image Analysis. The 2D images acquired during flow are analyzed using routines written in IDL (ITT Corporation, Boulder, CO). To obtain information about particle concentrations, we calculate the intensity as a function of position (x , y) averaged across all images within each image series. To correct for nonuniform illumination across the field of view, we normalize all averaged images by a bright-field image. To obtain information about the spatial arrangement of particles during flow, we use standard algorithms to locate the positions of the particles in two dimensions.³⁴ The short-range structure of the gels, as quantified by the nearest-neighbor distribution, does not undergo significant changes during flow.²⁶ We therefore characterize the long-range structure by calculating the neighbor density fluctuations (NDF),^{32,35} defined as $(\langle N^2 \rangle - \langle N \rangle^2) / \langle N \rangle$, as a function of box size L . In bulk systems, the NDF is related to the low-scattering-vector limit of the structure factor and is a measure of the isothermal compressibility of the material.³⁶ In the microscopic limit, probing the 3D NDF as a function of L explicitly measures the extent to which the extracted compressibility agrees with the macroscopic value.³⁵ Here, we employ the 2D NDF as a measure of the amount of heterogeneity in the long-length-scale structure of the system.

We quantify the flow properties of the suspension in two ways. Near the walls, particle displacements are small and we can directly apply standard algorithms³⁴ to calculate the particle trajectories. Near the center of the microchannel, however, the colloidal microspheres in our experiments move distances greater than the interparticle separation in consecutive frames and thus standard algorithms for tracking the positions of the particles cannot be used to calculate velocity profiles directly. Instead, the advection velocity across the microchannel is calculated using a modified 2D version of an algorithm used to analyze images of flowing colloidal glasses^{24,25,37,38} and gels.²⁶ Briefly, each image is subdivided into squares in which the velocity is nearly uniform. For

(28) van Blaaderen, A.; Vrij, A. *Langmuir* **1992**, *8*, 2921.

(29) Dickinson, E.; Eriksson, L. *Adv. Colloid Interface Sci.* **1991**, *34*, 1.

(30) Russel, W. B. *ACS Symp. Ser.* **1993**, *532*, 1.

(31) Lu, P. J.; Conrad, J. C.; Wyss, H. M.; Schofield, A. B.; Weitz, D. A. *Phys. Rev. Lett.* **2006**, *96*, 028306.

(32) Dibble, C. J.; Kogan, M.; Solomon, M. J. *Phys. Rev. E* **2006**, *74*, 041403.

(33) Xia, Y.; Whitesides, G. M. *Annu. Rev. Mater. Sci.* **1998**, *28*, 153.

(34) Crocker, J. C.; Grier, D. G. *J. Colloid Interface Sci.* **1996**, *179*, 298.

(35) Varadan, P.; Solomon, M. J. *Langmuir* **2003**, *19*, 509.

(36) Hansen, J. P.; McDonald, I. R. *Theory of Simple Liquids*, 2nd ed.; Academic Press: San Diego, CA, 1990.

(37) Isa, L.; Besseling, R.; Weeks, E. R.; Poon, W. C. K. *J. Phys.: Conf. Ser.* **2006**, *40*, 124.

(38) Besseling, R.; Weeks, E. R.; Schofield, A. B.; Poon, W. C. K. *Phys. Rev. Lett.* **2007**, *99*, 028301.

each pair of consecutive images $I_1(x, y)$ and $I_2(x, y)$, each square in the latter image is shifted by factors of Δx and Δy chosen to maximize the cross-covariance between $I_1(x, y)$ and $I_2(x + \Delta x, y + \Delta y)$. For each square, the 2D histogram of shift factors Δx and Δy over the entire image series exhibits a sharp maximum. We fit this histogram with a Gaussian and report the position of the center of the Gaussian as the advection velocity at position (x, y) .

Results and Discussion

We investigated the structure and velocity profiles of attractive colloidal suspensions flowing through microchannel constrictions, as shown in the schematic in Figure 1. In our experiments, the channel width narrows from a width D to a width d via a constriction with an opening angle of α . Surprisingly, we observed no significant differences in suspension structure between the two opening angles investigated. We thus report data only for $\alpha = 27^\circ$, whereas data for $\alpha = 72^\circ$ is provided as Supporting Information.

Averaged Measurements of Colloid Velocity and Distribution. To explore the effects of the constriction on the flow profiles of colloidal gels, we calculate the average advection velocity in the constriction regions using image correlation techniques. The average advection velocity increases downstream through the constriction region, as shown for a suspension with $\phi = 0.26$ flowing under an applied pressure of 0.7 kPa in a microchannel with $D/d = 2$ in Figure 2b; the increase in advection velocity in the outlet region is consistent with the conservation of particle flux. At the entrance to the constriction region is a region of reduced advection velocity. As the applied pressure is increased to 2.1 kPa, the average advection velocity increases throughout the channel and the decrease in average velocity due to the constriction entrance is somewhat mitigated (Figure 2a). Similar trends are seen for a larger turn-down ratio of $D/d = 3$. For an applied pressure of 0.7 kPa, the region of decreased velocity at the entrance to the constriction extends further downstream, as shown in Figure 2d; when the applied pressure is increased, this region of decreased velocity is again mitigated (Figure 2c). The entrance effect described here is most prominent for distances of less than $10 \mu\text{m}$ above the bottom surface of the microchannel; the size of the entrance region decreases near the midplane of the microchannel.

At the entrance to the constriction, the qualitative shape of the flow profile is a function of the applied pressure. When the applied pressure is relatively low, the flow profile is pluglike, as shown for a suspension with $\phi = 0.26$ flowing under an applied pressure of 0.7 kPa in a microchannel with $D/d = 2$ (the conditions shown in Figure 2b) in Figure 3a. We calculate the normalized Newtonian flow velocity,

$$\frac{U(x)}{U_{\max}} = \sum_{i \text{ odd}} (-1)^{(n-1)/2} \left[1 - \frac{\cosh(i\pi z/2L)}{\cosh(i\pi h/4L)} \right] \frac{\cos(i\pi x/2L)}{i^3}$$

where z is the distance from the midplane of the microchannel, L is the half-width of the channel, h is the microchannel height, and x is the lateral position across the channel.³⁹ Indeed, the flow profile in Figure 3a exhibits strong deviations from that expected for Newtonian flow. However, when the applied pressure is increased to 2.1 kPa, the flow profile is nearly Newtonian (Figure 3b). We observe a similar qualitative change in the flow profiles with increasing stress for a suspension flowing in a microchannel with $D/d = 3$ (Figure 3c,d). The qualitative change in the flow profiles with increasing applied pressure is consistent with prior observations of this system flowing through uniform microchannels.²⁶

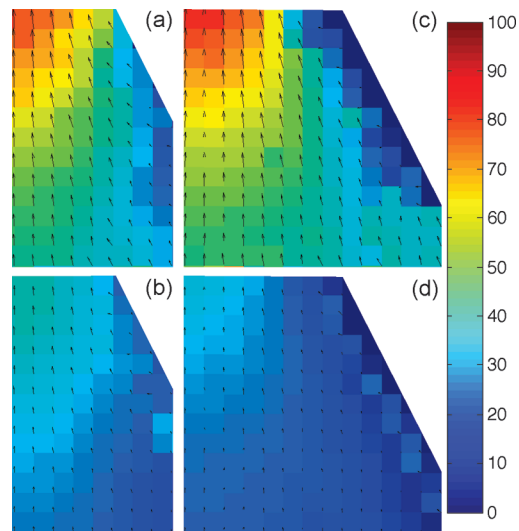


Figure 2. Reconstruction of flow profiles $9 \mu\text{m}$ above the bottom surface of the channel for suspensions flowing in devices with fixed $d = 50 \mu\text{m}$ and angle $\alpha = 27^\circ$ under applied pressures of (a, c) 2.1 kPa and (b, d) 0.7 kPa. (a, b) $D = 100 \mu\text{m}$ and (c, d) $D = 150 \mu\text{m}$. Colors and arrows indicate the magnitude and direction of velocity, respectively (given in $\mu\text{m/s}$ in colored bars). The block size is $32 \text{ pixels} \times 32 \text{ pixels}$ ($3.2 \times 3.2 \mu\text{m}^2$), and the suspension volume fraction is $\phi = 0.26$.

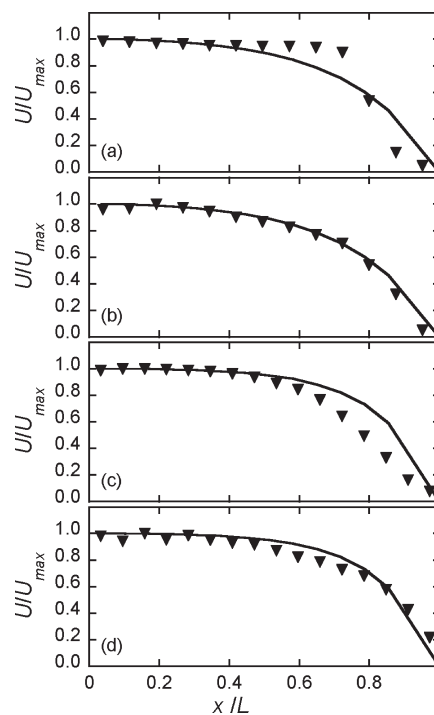


Figure 3. Normalized velocity U/U_{\max} as a function of normalized position across the channel x/L at the constriction entrance $9 \mu\text{m}$ above the bottom surface of the channel for the velocity profiles plotted in Figure 2 (symbols) and for a Newtonian fluid (solid lines). The origin ($x = 0$) is at the midpoint of the microchannel. Devices have fixed $d = 50 \mu\text{m}$ and angle $\alpha = 27^\circ$. (a, b) $D = 100 \mu\text{m}$; applied pressures are (a) 0.7 kPa and (b) 2.1 kPa. (c, d) $D = 150 \mu\text{m}$; applied pressures are (c) 0.7 kPa, and (d) 2.1 kPa. The suspension volume fraction is $\phi = 0.26$.

Downstream from the constriction, a significant change arises in the shear zone width w , defined as the distance from the wall at which the advection velocity is equal to $0.95V_c(h)$, where $V_c(h)$ is

(39) White, F. M. *Viscous Fluid Flow*, 3rd ed.; McGraw-Hill: Boston, 2006.

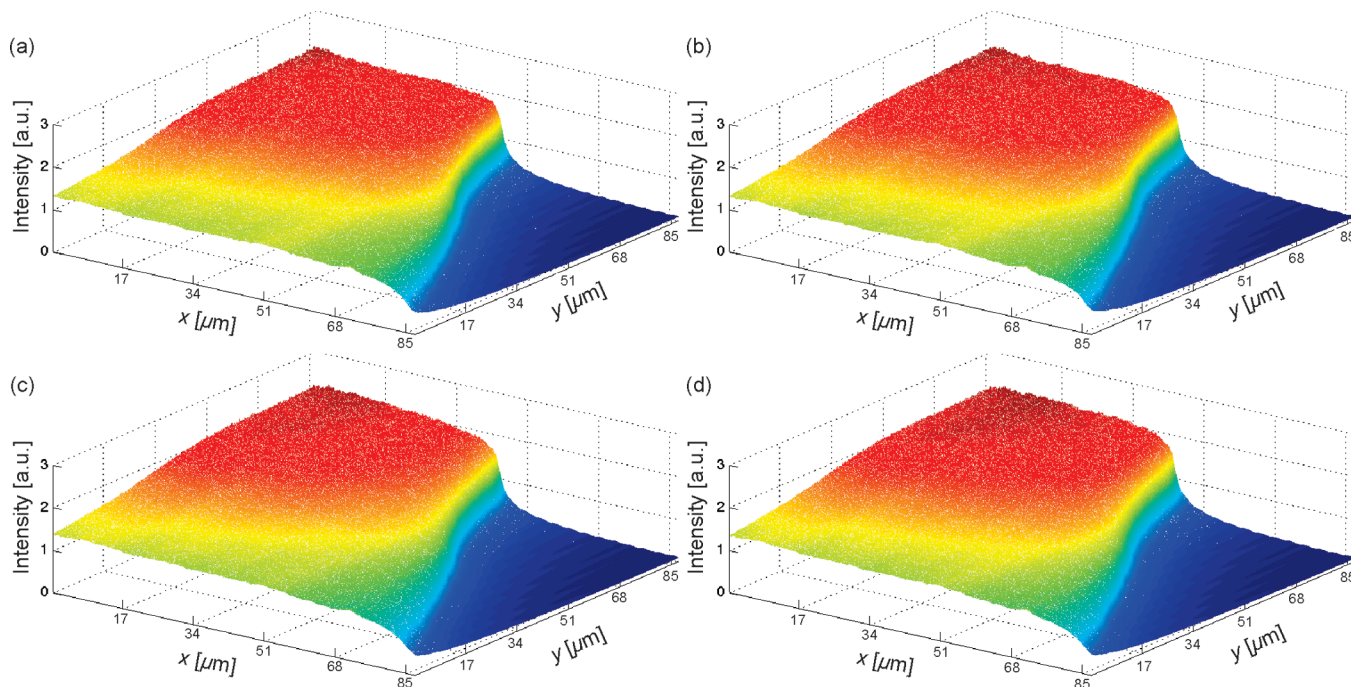


Figure 4. Three-dimensional representation of the intensity profile for a gel with $\phi = 0.26$ flowing through channels with $D = 150 \mu\text{m}$, $d = 50 \mu\text{m}$, and $\alpha = 27^\circ$ at a height of $9 \mu\text{m}$ above the bottom surface of the channel for applied pressures of (a) 0.7, (b) 2.1, (c) 4.1, and (d) 6.9 kPa. The origin of the (x, y) coordinate system used is shown in Figure 1. The image is $85 \mu\text{m} \times 85 \mu\text{m}$ in the x – y plane; the intensity is in arbitrary units. The suspension volume fraction is $\phi = 0.26$.

the maximum advection velocity at a height h above the bottom of the microchannel. For a suspension with $\phi = 0.26$ flowing under an applied pressure of 0.7 kPa in a microchannel with $D/d = 2$, we calculate $w_i \approx 36 \pm 3 \mu\text{m}$ ($\sim 0.72(D/2)$) at the channel inlet and $w_o \approx 24 \pm 2 \mu\text{m}$ ($\sim 0.96(d/2)$) at the channel outlet at a height $h = 3 \mu\text{m}$ above the bottom surface of the microchannel. For comparison, the expected shear zone width at the channel input for a Newtonian suspension is $w_{i,N} \approx 31 \mu\text{m}$ ($\sim 0.62(D/2)$) at a height of $h = 3 \mu\text{m}$. As h is increased to $15 \mu\text{m}$, the values of the shear zone width for the flowing suspension decrease somewhat to $w_i \approx 27 \mu\text{m}$ ($\sim 0.54(D/2)$) and $w_o \approx 18 \mu\text{m}$ ($\sim 0.72(d/2)$) (compared to the Newtonian value of $w_{i,N} \approx 32 \mu\text{m}$ ($\sim 0.64(D/2)$)). These calculations indicate that flow through a constriction increases the shear zone width, thereby leading to additional fluidization of the flow downstream. When the applied pressure is increased to 2.1 kPa, the shear zone width at the outlet ($w_o \approx 0.98(d/2)$) is again higher than at the inlet ($w_i \approx 0.77(D/2)$). At this applied pressure, w varies less strongly as a function of height, consistent with overall increased fluidization at higher shear rates. Similar trends are observed for a turn-down ratio of $D/d = 3$.

The change in shear zone width across the constriction implies that flow through the constriction changes the structure of the suspension. To quantify the effects of the constriction on the average distribution of particles, we calculate the average intensity during flow as a function of position within the constriction region. For a device with $D = 150 \mu\text{m}$, the averaged intensity in a series of images taken $9 \mu\text{m}$ above the bottom surface increases by roughly 60% downstream from the channel inlet to the channel outlet, as shown for a suspension flowing under an applied pressure of 0.7 kPa in Figure 4a. Averaged images of flow taken at higher applied pressures also show a markedly higher intensity at the channel output (Figure 4b–d), suggesting that the increase in intensity downstream does not simply reflect changes in particle velocity. Rather, the increased intensity reflects a slight increase in the concentration of the colloidal species at the outlet relative to

that at the inlet, which implies that the flow rates of the liquid and particles in the constriction must differ slightly. The averaged intensity images also reveal variations in particle distribution across the channels. Both at the channel inlet (small values of y in Figure 4) and at the outlet (large values of y) the intensity decreases from the center of the channel out to the lateral edge (small values of x). Finally, the intensity also increases with increasing height above the bottom wall of the microchannel, although this is a smaller effect than the downstream enhancement, with typical increases of 20–30%.

The increased intensity observed near the center of the microchannel reflects both the shear-enhanced migration⁴⁰ of clusters toward the center of the microchannel²¹ and the compression in streamlines induced by the constriction. Earlier experiments on flowing dense attractive suspensions showed that shear disrupts the network structure present during the quiescent state in two ways: by breaking the relatively weak bonds between clusters and by locally compacting clusters.^{41,42} Indeed, our earlier experiments on similar suspensions flowing in uniform microchannels revealed the formation of dense shear-induced clusters near the channel walls, where the shear stresses were highest.²⁶ The non-uniform shear stress exerted on these clusters drives their migration toward the center of the channel.⁴⁰

To determine the extent of segregation due to shear-induced migration, we estimate the entrance length over which the concentration profile develops. Previous experiments on colloidal hard-sphere suspensions reported entrance lengths of $L_e \approx O(100D)$, where D is the width of the microchannel, that increased with increasing Péclet number Pe .²² In our experiments, in which diffusion is greatly suppressed by the attractive interactions between the particles, we estimate²⁶ $Pe > 10^6$ and $D \approx O(100 \mu\text{m})$; using the

(40) Leighton, D.; Acrivos, A. *J. Fluid Mech.* **1987**, *181*, 415.

(41) Varadan, P.; Solomon, M. J. *J. Rheol.* **2003**, *47*, 943.

(42) Hoekstra, H.; Vermant, J.; Mewis, J. *Langmuir* **2003**, *19*, 9134.

results in ref 22, we estimate $L_c \approx 1-10$ cm, which is comparable to the inlet channel length of 2.5 cm. Thus, we expect to see an enhanced concentration near the center of the channel even prior to the constriction. By comparing the intensity at the center of the outlet to that at the center of the inlet, we estimate that the volume fraction in the center of the microchannel outlet is up to 30–40% higher than near the edges, which is somewhat larger than the enhancement seen for suspensions flowing at similar Pe in uniform microchannels.²¹ We conclude that the constriction induces an increase in concentration near the center of the channel that is greater than that predicted by shear-enhanced diffusion.

Measurements of average velocity and intensity indicate that the flow and structure of the suspension in the constriction region differ from those observed under both quiescent conditions and uniform microchannel flow. To investigate these differences in more detail, we analyze the structure and flow behavior on length scales associated with individual particles and with the clusters that they form.

Local Measurements of Jamming and Heterogeneity. The shear-zone width calculations indicate that flow through the constriction leads to greater fluidization downstream, yet the average advection velocities in the constriction region are relatively small. To reconcile these findings, we investigate the flow behavior in the sheared zone near the entrance of the constriction. We first directly visualize particle displacements by calculating the difference between consecutive images; particles with nearly zero displacements are uniformly dim, but particles with higher displacements have one bright edge and one dark edge. For a suspension with $\phi = 0.26$ flowing under an applied pressure of 0.7 kPa in a microchannel with $D/d = 2$, the difference images show that the particles near the entrance to the constriction have nearly zero displacements; by contrast, particles only a short distance from the walls exhibit much higher displacements (Figure 5a–d). The particles near the wall form a transiently jammed structure, around which other particles can still flow. The discontinuity visualized here is transient; at later times, even those particles immediately adjacent to the wall can be clearly seen to move (Supporting Information). Transient jamming likely arises from the weak van der Waals attraction between particles and the microchannel wall, which we estimate to be $\sim 13k_B T$ at a cutoff distance of 5 nm (corresponding to the polymer adlayer thickness⁴³) for PEI-coated silica microspheres of radius 430 nm interacting with a PDMS wall in a DMSO/water solution.⁴⁴

To characterize this transient jamming further, we explicitly calculate the particle velocities near the wall using standard particle-tracking algorithms.³⁴ Particles in the entrance region near the wall exhibit very low velocities (Figure 5e–h), and particles closer to the center of the microchannel exhibit higher velocities. Although the transition from nearly zero to finite velocity can be discontinuous in these regions, neighboring particles typically exhibit correlated motion on a length scale of $\sim 5-10$ particle diameters, thereby suggesting that the network yields at the boundaries between clusters.

Transient jamming behavior has also been observed in hard-sphere-like colloidal glasses;^{17,25} however, the origins of the jamming are different in these two systems. In hard-sphere-like glasses, periodic jamming arises from the interplay between shear thickening, which induces the formation of locally rarefied regions, and permeation flow, which erodes them. In that case, the periodicity may be related to the critical strain that must be accumulated before jamming can occur.²⁵ By contrast, in our

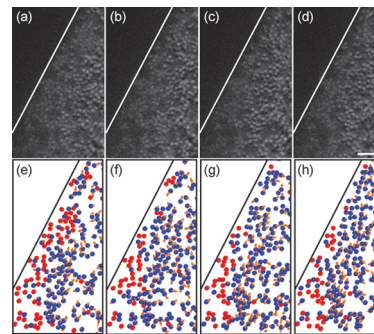


Figure 5. (a–d) Difference images illustrating particle displacements in a flowing suspension. Images are obtained by subtracting consecutive frames ($\Delta t = 1/30$ s). Scale bar: $5 \mu\text{m}$. (e–h) Particle positions (spheres) and velocities (arrows) for images in a–d. The particles with the smallest displacements are red. Applied pressure, 0.7 kPa; channel geometry, $d = 50 \mu\text{m}$; $D = 100 \mu\text{m}$; $\alpha = 27^\circ$, and suspension volume fraction, $\phi = 0.26$.

shear-thinning system, transient jamming arises from the yielding and reformation of bonds between colloidal particles and is not periodic: with limited statistics, we observe that the duration of a stagnation event ranges from ~ 0.5 to ~ 8 s whereas the interval between such events ranges from ~ 1 to ~ 15 s. In this system, yielding is determined by details of the local geometry, specifically, the local bond coordination number and cluster arrangement; thus, different configurations of particles may give rise to different yielding timescales.

Yielding at the boundaries between clusters provides one mechanism by which the shear modifies the long-length-scale structure of the suspension. We quantify the long-length-scale structure by calculating the number density fluctuations (NDF), $(\langle N^2 \rangle - \langle N \rangle^2) / \langle N \rangle$, over boxes of varying side length, L . For a quiescent gel with $\phi = 0.26$, the value of the NDF increases at the lowest values of a/L (Figure 6a). This dependence is characteristic of gels exhibiting cluster morphology,^{27,32} such as those formed via spinodal decomposition,^{45,46} and is also consistent with the structure observed in our earlier experiments on similar gels.²⁶

Changes in gel structure induced by flow can be captured by the NDF measurement. The value of the NDF for a suspension flowing through a constriction with $D/d = 2$ under an applied pressure of 0.7 kPa is generally greater than that of the quiescent suspension (Figure 6b), consistent with shear-induced clustering.⁴⁷ At a height of $3 \mu\text{m}$ above the bottom wall of the microchannel, the value of the NDF of the flow decreases monotonically with decreasing a/L ; by contrast, at a height of $12 \mu\text{m}$ above the bottom surface the value of the NDF increases with decreasing a/L at the lowest values of a/L . These features suggest that the high shear rates near the wall lead to an increase in the number of voids, consistent with the disruption of the gel structure into single particles or smaller clusters. By contrast, the relatively low shear rates near the midplane of the channel are insufficient to disrupt the gel structure at this applied pressure.

Further increases in the applied pressure disrupt the gel structure even in the center of the channel. For a gel flowing under an applied pressure of 4.1 kPa through the same turndown ratio, the value of the NDF $3 \mu\text{m}$ above the bottom wall of the microchannel is comparable to that measured at 0.7 kPa for all a/L (Figure 6c) and also monotonically decreases with decreasing a/L . However, at a height of $12 \mu\text{m}$ above the bottom wall the value of

(43) Carpineti, M.; Giglio, M. *Phys. Rev. Lett.* **1992**, *68*, 3327.

(44) Lu, P. J.; Zaccarelli, E.; Ciulla, F.; Schofield, A. B.; Sciortino, F.; Weitz, D. A. *Nature* **2008**, *453*, 499.

(45) Vermant, J.; Solomon, M. J. *J. Phys.: Condens. Matter* **2005**, *17*, R187.

(43) Yoshikawa, J.; Lewis, J. A.; Chun, B.-W. *J. Am. Ceram. Soc.* **2009**, *92*, S42.

(44) Israelachvili, J. N. *Intermolecular and Surface Forces*, 2nd ed.; Academic Press: Amsterdam, 1991.

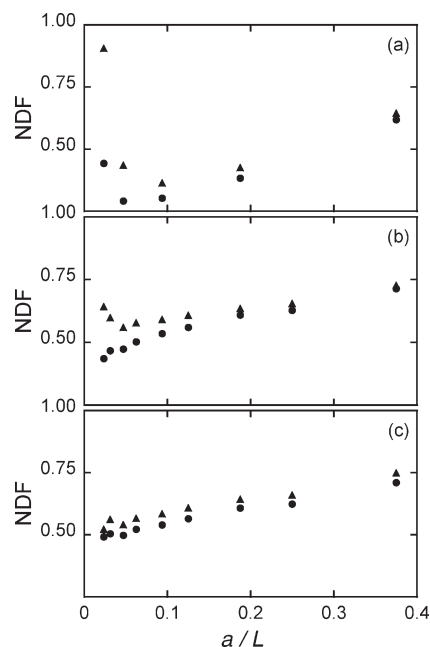


Figure 6. Number density fluctuations (NDF), $(\langle N^2 \rangle - \langle N \rangle^2) / \langle N \rangle$, as a function of block size length a/L for (a) a quiescent suspension and (b, c) suspensions flowing under applied pressures of (b) 0.7 kPa and (c) 4.1 kPa in a microchannel with $d = 50 \mu\text{m}$, $D = 100 \mu\text{m}$, and $\alpha = 27^\circ$. Symbols in all graphs indicate the height above the bottom surface: (●) $3 \mu\text{m}$ and (▲) $12 \mu\text{m}$. The suspension volume fraction is $\phi = 0.26$.

the NDF also monotonically decreases, in contrast to the slight increase seen at the lowest values of a/L at the lower applied pressure. These data suggest that the increase in structural heterogeneity with applied pressure arises from the partial disruption of the gel network into clusters and single particles; this observation is consistent with our earlier work on flow in uniform microchannels.²⁶ To confirm this, we estimate the strain rate across the microchannel to be $\dot{\gamma} = V_c/(h/2) \approx 20 \text{ s}^{-1}$, where $V_c \approx 400 \mu\text{m/s}$ is the velocity measured near the center of the microchannel and h is the microchannel height, which is comparable to the critical strain measured via bulk rheology, $\dot{\gamma}_c \approx 40 \text{ s}^{-1}$ (Supporting Information).

We also calculate a spatially resolved NDF as a function of position across the channel. For an applied pressure of 0.7 kPa, the value of the NDF calculated using a box size of $L = 32$ pixels ($a/L = 0.094$) is nearly constant across the center of the microchannel outlet and increases slightly near the lateral wall of the microchannel (Figure 7a). Smaller values of box size L also give rise to this increase in the NDF near the lateral walls; moreover, the width of the zone of increase, estimated as L times the number of points, is independent of L . Collectively, these observations indicate an increase in the number of voids on multiple length scales. Surprisingly, the value of the NDF is not a strong function of the height above the bottom surface of the microchannel, as can be seen by comparing the data for 3 and $12 \mu\text{m}$. We obtain similar results for the value of NDF at a higher applied pressure (Figure 7b), with a slightly greater enhancement in the NDF seen at the lateral wall, and for all values of L . These data suggest that the disruption of the network structure results from the change in streamlines induced by the constriction.

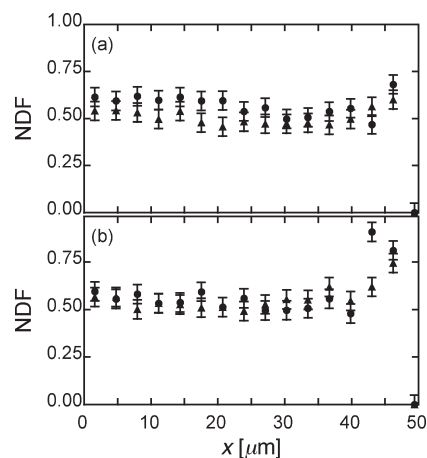


Figure 7. Number density fluctuations (NDF), $(\langle N^2 \rangle - \langle N \rangle^2) / \langle N \rangle$, as a function of lateral position x at the outlet for suspensions flowing under an applied pressure of (a) 0.7 kPa and (b) 4.1 kPa in a microchannel with $d = 50 \mu\text{m}$, $D = 100 \mu\text{m}$, and $\alpha = 27^\circ$. Data are measured $100 \mu\text{m}$ downstream from constriction. Box size L used in these calculations is 32 pixels ($a/L = 0.094$). Symbols in all graphs indicate the height above the bottom surface. Flowing suspensions: (●) $3 \mu\text{m}$ and (▲) $12 \mu\text{m}$. The suspension volume fraction is $\phi = 0.26$.

Conclusions

We show that flow through microchannel constrictions leads to pronounced structural changes within attractive colloidal suspensions. First, the particle concentration increases slightly as the suspension flows through the constriction, consistent with filter pressing. Second, flow through the constriction disrupts the network structure through yielding at intracuster boundaries. The averaged bulk flow profiles for such suspensions are smooth: when the applied shear stress is sufficiently small, plug flow occurs near the center of the microchannel, whereas at higher applied shear stresses the flow profile is fluidlike. We further observe transient jamming events close to the walls, related to the development of a stagnation zone near the entrance of the constriction in which particles repeatedly jam and unjam via aggregation and shear-induced yielding. These transient jamming and unjamming events further disrupt the local structure, leading to increased fluidization downstream from the constriction.

Acknowledgment. This work was supported by the NSF Center for Directed Assembly of Nanostructures (grant no. DMR-0642573). We gratefully acknowledge B. Wrestler for assistance with device fabrication and R. F. Shepherd for assistance in preparing the schematic image.

Supporting Information Available: Rheology of colloidal gel samples used in flow experiments. Three-dimensional representation of the intensity profile for the flow of a gel. Intensity profiles across the channel at the constriction outlet. Number density fluctuations as a function of position across the channel at the constriction inlet and outlet. Shear zone width w/L calculated at channel inlets and outlets. Movies of colloidal gels flowing through microchannels. This material is available free of charge via the Internet at <http://pubs.acs.org>.